

# Joint Active and Passive Beamforming for IRS-Assisted Multi-User MIMO Systems: A VAMP Approach

Haseeb Ur Rehman, Faouzi Bellili, *Member, IEEE*, Amine Mezghani, *Member, IEEE*, and Ekram Hossain, *Fellow, IEEE*

## Abstract

This paper tackles the problem of joint active and passive beamforming optimization for an intelligent reflective surface (IRS)-assisted multi-user downlink multiple-input multiple-output (MIMO) communication system. We aim to maximize spectral efficiency of the users by minimizing the mean square error (MSE) of the received symbol. For this, a joint optimization problem is formulated under the minimum mean square error (MMSE) criterion. First, block coordinate descent (BCD) is used to decouple the joint optimization into two sub-optimization problems to separately find the optimal active precoder at the base station (BS) and the optimal matrix of phase shifters for the IRS. While the MMSE active precoder is obtained in a closed form, the optimal phase shifters are found iteratively using a modified version (also introduced in this paper) of the vector approximate message passing (VAMP) algorithm. We solve the joint optimization problem for two different models for IRS phase shifts. First, we determine the optimal phase matrix under a unimodular constraint on the reflection coefficients, and then under the constraint when the IRS reflection coefficients are modeled by a reactive load, thereby validating the robustness of the proposed solution. Numerical results are presented to illustrate the performance of the proposed method using multiple channel configurations. The results validate the superiority of the proposed solution as it achieves higher throughput compared to state-of-the-art techniques.

## Index Terms

Intelligent reflective surface (IRS), IRS-assisted multi-user MIMO, joint active and passive beamforming, vector approximate message passing (VAMP) optimization

The authors are with the Department of Electrical and Computer Engineering at the University of Manitoba, Canada (emails: [urrehmah@myumanitoba.ca](mailto:urrehmah@myumanitoba.ca), [{Faouzi.Bellili, Amine.Mezghani, Ekram.Hossain}@umanitoba.ca](mailto:{Faouzi.Bellili, Amine.Mezghani, Ekram.Hossain}@umanitoba.ca)).

## I. INTRODUCTION

### A. Background

The need for higher data rates in wireless communication is soaring. This calls for innovative and economically viable communication technologies that can keep up with the increasing network capacity requirement. Massive multiple-input multiple-output (MIMO) technology can fulfill the network capacity requirement for beyond fifth-generation (B5G) wireless networks [1]–[3]. The basic idea of massive MIMO is to equip the base stations (BSs) with tens (if not hundreds) of antenna elements so as to simultaneously serve multiple mobile devices using the same time/frequency resources. Despite the advantages of massive MIMO, its practical large-scale deployment is hindered by high hardware cost and energy consumption [4], [5]. Moreover, although high-frequency bands such as millimeter wave (mmWave) benefit from massive MIMO, its maximum potential is still often not utilized in a practical scenario with many blockages between the BS and the mobile device due to its less penetrative propagation characteristic [6].

One promising technology that has been introduced recently is intelligent reflective surfaces (IRSs), also called reconfigurable intelligent surfaces (RISs) [7], [8]. IRS is composed of a planar metasurface consisting of a large number of passive reflective elements. Moreover, IRS does not require a power amplifier for transmission which makes it an energy-efficient technology. This allows the IRS to passively modify the propagation of the signal by reconfiguring the phases of its reflective elements through a controller attached to the surface [9]. Therefore, IRSs can be utilized to perform passive beamforming (i.e., by only optimizing the IRS phases without actively powering IRS antenna elements as opposed to active beamforming at the BS) to improve the received signal power while reducing the interference for unintended users, thereby enhancing the overall throughput of the network [10]. Practically, IRS deployment requires a large number of cost-effective phase shifters (PSs) on a surface that can be easily integrated into a traditional wireless network [11]. Due to aforementioned reasons, IRS has gained substantial research interest in the wireless research community over the recent few years. [10]–[18].

In [14], a single-user multiple-input single-output (MISO) wireless system assisted by multiple IRSs in the downlink configuration is studied. While making use of statistical channel state information (CSI) only, the optimal reflective coefficients are calculated using a stochastic convex approximation method. In [19], an IRS-assisted multi-cluster MISO system serving multiple users is considered wherein the authors seek to minimize the transmit power under a minimum signal-

to-interference-plus-noise ratio (SINR) constraint by jointly optimizing IRS phase shifts and transmit precoding. They tackle the underlying problem through alternating direction method of multipliers (ADMM). An IRS-aided MISO and MIMO system with discrete phase shifts for IRS elements is also discussed in [12]. The authors formulate the problem of minimizing the transmit power under minimum SINR constraint and jointly optimize the transmit precoding and IRS phase shifts in a mixed-integer non-linear programming framework. In [17], a relatively more practical model for IRS reflection coefficients is considered and then a penalty-based algorithm is used to find the optimal phase matrix.

The vast majority of the existing work considers a MISO wireless system assisted by a single or multiple IRSs serving a single user [13], [14], [14]–[17]. So far, limited research has been conducted on IRS-aided multi-user MIMO systems. Moreover, IRS reflection coefficients are often modeled as ideal phase shifters and a realistic approach towards modeling reflection coefficients has rarely been investigated. In fact, most of the existing methods are limited to a single-phase shifter model, unimodular phase shifts being the most common one, and hence they are not robust to accommodate various hardware impairments for reflection coefficients [13]–[17].

### *B. Contributions*

In this paper, we consider a multi-user IRS-assisted single-cell downlink MIMO system with a single IRS. The IRS is equipped with a large number of passive phase shifters that aid the BS to serve a small number of users. We propose a robust solution for the problem of jointly optimizing the active and passive beamforming tasks under different models for the IRS reflection coefficients and propose a robust solution. The main contributions embodied by this paper are as follows:

- We minimize the mean square error (MSE) of the received symbol and thereby maximizing the spectral efficiency of the users by jointly optimizing the transmit precoding matrix and the reflection coefficients at the IRS. To that end, we first formulate the joint optimization problem under the MMSE criterion in order to minimize the MSE of the received signals for all users at the same time.
- To solve the underlying joint optimization problem, we first split it using alternate optimization block coordinate descent (BCD) [20] into two simpler sub-optimization problems to separately optimize the active precoder at the BS and the reflection coefficients at the

IRS. The precoding sub-optimization problem is similar to the MMSE transmit precoding optimization for a traditional MIMO system, which can be solved in closed form through Lagrange optimization.

- We modify and extend the existing VAMP algorithm [21] and propose a robust technique for finding optimal reflective coefficients for the IRS under multiple constraints. Precisely, we find the optimal phase matrix under two different models for the reflection coefficients: *i*) Under the unimodular constraint on the IRS reflection coefficients and *ii*) under a realistic constraint, where each IRS element is terminated by a tunable simple reactive load.
- We provide the order of complexity of the proposed solution.
- We present various numerical results to compare the proposed solution with a standalone massive MIMO system using maximal ratio transmission (MRT) precoder and an ADMM-based solution. The results show that, the proposed solution: *i*) achieves higher throughput than massive MIMO system while using a significantly smaller number of transmit antennas, and *ii*) outperforms the ADMM-based solution in terms of throughput in less time while using the same resources.

### C. Paper Organization and Notations

The rest of the paper is organized as follows: the system model along with the problem formulation for jointly optimizing the active precoder and the reflection coefficients are discussed in Section II. Section III briefly introduces the VAMP algorithm and then extends it to solve optimization problems. In Section IV, we solve the joint optimization problem at hand using the proposed extended version of VAMP. In Section V, we further the underlying joint optimization problem under the “simple reactive loading” constraint on the IRS phase shifts. Numerical results for the proposed solution are shown in Section VI.

**Notations:** Lowercase letters (e.g.,  $r$ ) denote scalar variables. The uppercase italic letters (e.g.,  $N$ ) represent scalar constants. Vectors are denoted by small boldface letters (e.g.  $\mathbf{z}$ ) and the  $k$ -th element of  $\mathbf{z}$  is denoted as  $z_k$ . Exponent on a vector (e.g.,  $\mathbf{z}^n$ ) denotes component-wise exponent on every element of the vector. Capital boldface letters (e.g.,  $\mathbf{A}$ ) are used to denote matrices  $a_{ik}$  and  $\mathbf{a}_i$  stand, respectively, for the  $(i, k)$ -th entry and the  $i$ -th column of  $\mathbf{A}$ .  $\mathbb{C}^{M \times N}$  denotes the set of matrices of size  $M \times N$  with complex elements and  $\mathbf{A}^{-k}$  means  $(\mathbf{A}^{-1})^k$ .  $\text{Rank}(\mathbf{A})$ ,  $\text{Tr}(\mathbf{A})$ , return, respectively, the Rank and the trace of any matrix  $\mathbf{A}$ . We also use  $\|\cdot\|_2$ ,  $\|\cdot\|_{\text{F}}$ ,  $(\cdot)^*$ ,  $(\cdot)^T$ ,  $(\cdot)^H$  to denote the  $\mathcal{L}_2$  norm, Frobenius norm, the conjugate, the transpose,

and the conjugate transpose operators, respectively. The operator  $\langle \cdot \rangle$  returns the mean of the elements/entries of any vector or matrix. Moreover,  $\text{vec}(\cdot)$  and  $\text{unvec}(\cdot)$  denote vectorization of matrix and unvectorization of a vector back to its original matrix form, respectively.  $\text{Diag}(\cdot)$  operates on a vector and generates a diagonal matrix by placing that vector in the diagonal. The statistical expectation is denoted as  $\mathbb{E}\{\cdot\}$ . An independent and identically distributed (i.i.d) random vector with complex normal distribution is represented by  $\mathbf{x} \sim \mathcal{CN}(\mathbf{x}; \mathbf{u}, \gamma^{-1}\mathbf{I})$ , where  $\mathbf{u}$  and  $\gamma^{-1}$  denote its mean and variance, respectively. The imaginary unit is represented by  $j = \sqrt{-1}$ . The proportional relationship between any two entities (functions or variables) is represented by  $\propto$  operator. Lastly, the operators  $\otimes$  and  $\odot$  denote the Kronecker and Hadamard product, respectively.

## II. SYSTEM MODEL, ASSUMPTIONS, AND PROBLEM FORMULATION

Consider a BS that is equipped with  $N$  antenna elements serving  $M$  ( $M < N$ ) single-antenna users in the downlink. The BS is assisted by an IRS which has  $K$  ( $K > M$ ) reflective elements. For each user, we have a direct link to the BS expressed by a channel vector  $\mathbf{h}_{b-u} \in \mathbb{C}^{N \times 1}$ . The channel of the IRS-user link is denoted by  $\mathbf{h}_{s-u} \in \mathbb{C}^{N \times 1}$ . Let  $\mathbf{H}_{b-s} \in \mathbb{C}^{K \times N}$  denote the channel matrix of the MIMO IRS-BS link. The signal received at the IRS is phase-shifted by a diagonal matrix  $\mathbf{\Upsilon} = \text{Diag}(v_1, v_2 \dots, v_K) \in \mathbb{C}^{K \times K}$  with unimodular diagonal entries, i.e.,  $|v_k| = 1$  for  $k = 1, \dots, K$ . In other words, for each reflection element, we have  $v_k = e^{j\theta_k}$  for some phase shift  $\theta_k \in [0, 2\pi]$ . The received signal for user  $m$  can be expressed as follows:

$$y_m = \alpha \left( \mathbf{h}_{s-u,m}^H \mathbf{\Upsilon} \mathbf{H}_{b-s} \sum_{m'=1}^M \mathbf{f}_{m'} \mathbf{s}_{m'} + \mathbf{h}_{b-u,m}^H \sum_{m'=1}^M \mathbf{f}_{m'} \mathbf{s}_{m'} + \mathbf{w} \right), \quad m = 1, \dots, M, \quad (1)$$

where  $\mathbf{s}_m \sim \mathcal{CN}(s; 0, 1)$  is the unknown transmit symbol,  $\mathbf{w} \sim \mathcal{CN}(w; 0, \sigma_w^2)$  denotes additive white Gaussian noise (AWGN), and  $\alpha \in \mathbb{R}$  refers to the scalar pre-processing at the receiver. Here,  $\mathbf{f}_m \in \mathbb{C}^{N \times 1}$  are the precoding vector that are used for power allocation and beamforming purposes. Let  $\mathbf{F} = [\mathbf{f}_1, \mathbf{f}_2, \dots, \mathbf{f}_M]$  be the precoding matrix and let  $P$  denote the total transmit power then  $\mathbb{E}\{\|\mathbf{F}\mathbf{s}\|^2\} = P$ . Let  $\mathbf{H}_{b-u} = [\mathbf{h}_{b-u,1}, \mathbf{h}_{b-u,2}, \dots, \mathbf{h}_{b-u,M}]$  and  $\mathbf{H}_{s-u} = [\mathbf{h}_{s-u,1}, \mathbf{h}_{s-u,2}, \dots, \mathbf{h}_{s-u,M}]$ . Then, by stacking all the users' signals in one vector  $\mathbf{y} = [y_1, y_2, \dots, y_M]^T$ , we can express the input-output relationship of the multi-user MIMO system as:

$$\mathbf{y} = \alpha \left( \underbrace{\mathbf{H}_{s-u}^H \mathbf{\Upsilon} \mathbf{H}_{b-s} \mathbf{F} \mathbf{s}}_{\text{Users-IRS-BS}} + \underbrace{\mathbf{H}_{b-u}^H \mathbf{F} \mathbf{s}}_{\text{Users-BS}} + \mathbf{w} \right). \quad (2)$$

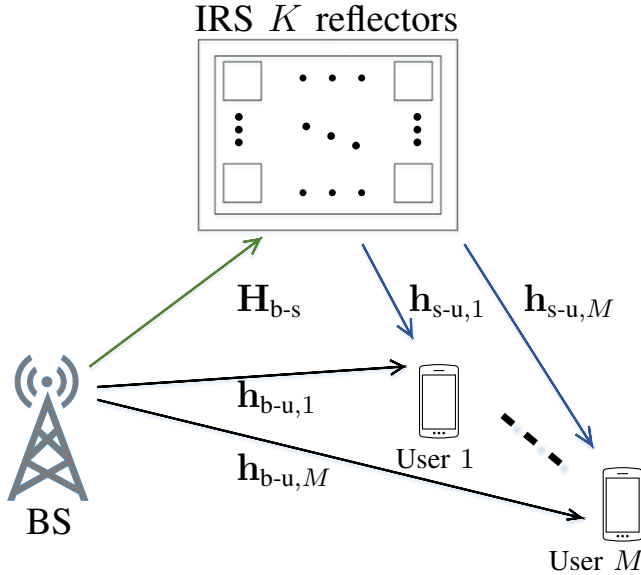


Fig. 1: IRS-assisted multi-user MIMO system.

The overall effective channel matrix for all users thus given by:

$$\mathbf{H}^H = \mathbf{H}_{s-u}^H \mathbf{\Upsilon} \mathbf{H}_{b-s} + \mathbf{H}_{b-u}^H. \quad (3)$$

Moreover, we assume that the channel state information (CSI) for all the channels is perfectly known at the BS. Denoting the SINR experienced by user  $m$  as  $\rho_m$ , the associated spectral efficiency is given by:

$$C_m = \log_2(1 + \rho_m). \quad (4)$$

We aim to minimize the received symbol error of each user under the MMSE criterion, which consequently maximizes user SINR. In fact According to the I-MMSE relationship [22], [23], the SINR of each  $m$ -th user is inversely proportional to the MMSE of its received symbol:

$$1 + \rho_m = \frac{1}{\text{MMSE}_m}. \quad (5)$$

Subsequently, the spectral efficiency for user  $m$  can be expressed as:

$$C_m^{\text{MMSE}} = \log_2 \left( \frac{1}{\text{MMSE}_m} \right). \quad (6)$$

The MSE of the received symbol for user  $m$  is given by  $\mathbb{E}_{y_m, s_m} \{ |y_m - s_m|^2 \}$ , and for  $M$  users, the sum symbol MSE can be written as:

$$\sum_{i=1}^M \mathbb{E}_{y_i, s_i} \{ |y_i - s_i|^2 \} = \mathbb{E}_{\mathbf{y}, \mathbf{s}} \{ \|\mathbf{y} - \mathbf{s}\|_2^2 \}. \quad (7)$$

Thus, our problem under the MMSE criterion can be formulated as follows:

$$\arg \min_{\alpha, \mathbf{F}, \mathbf{Y}} \mathbb{E}_{\mathbf{y}, \mathbf{s}} \{ \|\mathbf{y} - \mathbf{s}\|_2^2 \}, \quad (8a)$$

$$\text{subject to } \mathbb{E}_{\mathbf{s}} \{ \|\mathbf{F}\mathbf{s}\|_2^2 \} = P, \quad (8b)$$

$$v_{ik} = 0, \quad i \neq k, \quad (8c)$$

$$|v_{ii}| = 0, \quad i = 1, 2, \dots, K. \quad (8d)$$

Note that the objective function in (8a) ensures that the MSE is minimized for each user and hence the spectral efficiency is maximized for each user. We take expectation involved in (8a) and (8b) with respect to (w.r.t.) the random vectors  $\mathbf{s}$  and  $\mathbf{w}$  and thereby leading to:

$$\arg \min_{\alpha, \mathbf{F}, \mathbf{Y}} \|\alpha \mathbf{H}^H \mathbf{F} - \mathbf{I}_M\|_F^2 + M\alpha^2 \sigma_w^2, \quad (9a)$$

$$\text{s.t. } \|\mathbf{F}\|_F^2 = P, \quad (9b)$$

$$v_{ik} = 0, \quad i \neq k, \quad (9c)$$

$$|v_{ii}| = 0, \quad i = 1, 2, \dots, K. \quad (9d)$$

The problem in (9) is a non-convex optimization problem due to the unimodular constraint on in (9d). Furthermore, later in this paper, we will solve the same problem under another constraint on the reflection coefficients. VAMP is a low-complexity iterative algorithm that can be utilized to solve optimization problems and we will show that it can efficiently handle different constraints on the optimization variables. One could also envisage the use of ADMM, which is a penalty-based iterative algorithm for solving constrained optimization problems. However, it is shown in [24] that VAMP converges faster than ADMM because of its automatic tuning of the required parameters.

### III. MODIFIED VAMP ALGORITHM FOR CONSTRAINED OPTIMIZATION

Recently, message passing algorithms [21], [25], [26] have gained attention in estimation theory because of their high performance, fast convergence. Vector approximate message passing (VAMP) [21] is a low-complexity algorithm that solves quadratic loss optimization of recovering a vector from noisy linear measurements. In this section, we briefly discuss the standard max-sum VAMP algorithm and we modify it to solve constrained optimization problems for matrices involving linear mixing.

### A. Background on Max-Sum VAMP

Approximate message passing (AMP)-based computational techniques have gained a lot of attention since their introduction within the compressed sensing framework [25]. To be precise, AMP solves the standard linear regression problem of recovering a vector  $\mathbf{x}_0 \in \mathbb{C}^N$  from noisy linear observations:

$$\mathbf{z} = \mathbf{A}\mathbf{x}_0 + \mathbf{w}, \quad (10)$$

where  $\mathbf{A} \in \mathbb{C}^{M \times N}$  (with  $M \ll N$ ) is called sensing matrix and  $\mathbf{w} \sim \mathcal{CN}(0, \gamma_w^{-1}\mathbf{I}_M)$ , with  $\gamma_w > 0$ , so  $p_{\mathbf{z}|\mathbf{x}}(\mathbf{z}|\mathbf{x}) = \mathcal{CN}(\mathbf{z}; \mathbf{A}\mathbf{x}, \gamma_w^{-1}\mathbf{I}_M)$ . Interestingly, the performance of AMP under independent and identically distributed (i.i.d.) Gaussian sensing matrices,  $\mathbf{A}$ , can be rigorously tracked through scalar state evolution (SE) equations [27]. One major drawback of AMP, however, is that it often diverges if the sensing matrix,  $\mathbf{A}$ , is ill-conditioned or has a non-zero mean. To circumvent this problem, vector AMP (VAMP) algorithm was proposed and rigorously analyzed through SE equations in [21]. Although there is no theoretical guarantee that VAMP will always converge, strong empirical evidence suggests that VAMP is more resilient to badly conditioned sensing matrices given that they are right-orthogonally invariant [21]. Consider the joint probability distribution function (pdf) of  $\mathbf{x}$  and  $\mathbf{z}$ ,  $p_{\mathbf{x},\mathbf{z}}(\mathbf{x}, \mathbf{z})$ , as follows:

$$p_{\mathbf{x},\mathbf{z}}(\mathbf{x}, \mathbf{z}) = p_{\mathbf{x}}(\mathbf{x}) \mathcal{CN}(\mathbf{z}; \mathbf{A}\mathbf{x}, \gamma_w^{-1}\mathbf{I}_M). \quad (11)$$

Here  $p_{\mathbf{x}}(\mathbf{x})$  is some prior distribution on the vector  $\mathbf{x}$  whose elements are assumed to be i.i.d. vector with a common prior distribution,  $p_{\mathbf{x}}(x)$ , as follows:

$$p_{\mathbf{x}}(\mathbf{x}) = \prod_{i=1}^N p_{\mathbf{x}}(x_i). \quad (12)$$

Thus, max-sum VAMP solves the following optimization problem:

$$\hat{\mathbf{x}} = \arg \min_{\mathbf{x}} \|\mathbf{z} - \mathbf{A}\mathbf{x}\|^2, \quad (13)$$

by finding the *maximum a posteriori* (MAP) estimate of  $\mathbf{x}_0$  as follows:

$$\hat{\mathbf{x}} = \arg \max_{\mathbf{x}} p_{\mathbf{x}|\mathbf{z}}(\mathbf{x}|\mathbf{z}). \quad (14)$$

The algorithm consists of the following two modules.

1) *MAP/LMMSE Estimator*: At iteration  $t$ , the MAP estimator receives extrinsic information (message) from the separable (i.e., element-wise) MAP denoiser of  $\mathbf{x}$  in the form of a mean vector,  $\mathbf{r}_{t-1}$ , and a scalar variance,  $\gamma_{t-1}^{-1}$ , and computes the MAP estimate and the associated posterior variance from the linear observations,  $\mathbf{z} = \mathbf{Ax} + \mathbf{w}$ , by using a Gaussian prior,  $\mathcal{CN}(\mathbf{x}; \mathbf{r}_{t-1}, \gamma_{t-1}^{-1} \mathbf{I}_N)$ , on  $\mathbf{x}$ . Because we are dealing with Gaussian densities, the MAP estimate is equal to the Linear MMSE (LMMSE) and given as follows:

$$\bar{\mathbf{x}}_t = (\gamma_w \mathbf{A}^H \mathbf{A} + \gamma_{t-1} \mathbf{I}_N)^{-1} (\gamma_w \mathbf{A}^H \mathbf{z} + \gamma_{t-1} \mathbf{r}_{t-1}), \quad (15)$$

and its posterior variance is given by:

$$\bar{\gamma}_t^{-1} = \frac{1}{N} \text{Tr} \left( [\gamma_w \mathbf{A}^H \mathbf{A} + \gamma_{t-1} \mathbf{I}_N]^{-1} \right). \quad (16)$$

The extrinsic information on  $\mathbf{x}$  is updated as follows:

$$\mathcal{CN}(\mathbf{x}; \bar{\mathbf{x}}_t, \bar{\gamma}_t^{-1} \mathbf{I}_N) / \mathcal{CN}(\mathbf{x}; \mathbf{r}_{t-1}, \gamma_{t-1}^{-1} \mathbf{I}_N),$$

and then sent back in the form of mean vector,  $\tilde{\mathbf{r}}_t = (\bar{\mathbf{x}}_t \bar{\gamma}_t - \mathbf{r}_{t-1} \gamma_{t-1}) / (\bar{\gamma}_t - \gamma_{t-1})$ , and a scalar variance,  $\tilde{\gamma}_t^{-1} = (\bar{\gamma}_t - \gamma_{t-1})^{-1}$ , to the separable MAP denoiser of  $\mathbf{x}$ . The SVD (singular value decomposition) form of VAMP directly computes extrinsic mean vector  $\tilde{\mathbf{r}}_t$  and scalar variance  $\tilde{\gamma}_t^{-1}$ , and can be readily obtained by substituting  $\mathbf{A} = \mathbf{U} \text{Diag}(\boldsymbol{\omega}) \mathbf{V}^H$  in (15) and (16).

2) *MAP Estimator of  $\mathbf{x}$* : This module computes the MAP estimate,  $\hat{\mathbf{x}}_t$ , of  $\mathbf{x}$  from the joint distribution  $p_{\mathbf{x}}(\mathbf{x}) \mathcal{CN}(\mathbf{x}; \tilde{\mathbf{r}}_t, \tilde{\gamma}_t^{-1} \mathbf{I}_N)$ . Because  $\mathbf{x}$  is i.i.d., the MAP estimator, also called denoiser function, is separable. It is expressed as:

$$\hat{x}_{i,t} = g_{1,i}(\tilde{r}_{i,t}, \tilde{\gamma}_t) \triangleq \arg \max_{x_i} [-\tilde{\gamma}_t |x_i - \tilde{r}_{i,t}|^2 + \ln p_{\mathbf{x}}(x_i)], \quad (17)$$

or equivalently,

$$g_{1,i}(\tilde{r}_{i,t}, \tilde{\gamma}_t) = \arg \min_{x_i} [\tilde{\gamma}_t |x_i - \tilde{r}_{i,t}|^2 - \ln p_{\mathbf{x}}(x_i)]. \quad (18)$$

The derivative of the scalar MAP denoiser w.r.t.  $\tilde{r}_i$  is given by [21]:

$$g'_{1,i}(\tilde{r}_{i,t}, \tilde{\gamma}_t) = \tilde{\gamma}_t \hat{\gamma}_t, \quad (19)$$

where  $\hat{\gamma}_t$  is the posterior precision. Similar to LMMSE module, the denoiser module computes extrinsic mean vector,  $\mathbf{r}_t = (\hat{\mathbf{x}}_t \hat{\gamma}_t - \tilde{\mathbf{r}}_t \tilde{\gamma}_t) / (\hat{\gamma}_t - \tilde{\gamma}_t)$ , and scalar variance,  $\gamma_t^{-1} = (\hat{\gamma}_t - \tilde{\gamma}_t)^{-1}$ , and sends them back to the LMMSE module for the next iteration. The process is repeated until convergence.

A major advantage of VAMP is that it decouples the prior information,  $p_{\mathbf{x}}(\mathbf{x})$ , and the observations,  $p_{\mathbf{x}|\mathbf{z}}(\mathbf{z}|\mathbf{x})$ , into two separate modules. Moreover, it also enables the denoiser function to be separable even if the elements of  $\mathbf{x}$  are correlated in which case the LMMSE module can easily incorporate such correlation information. The steps of the standard max-sum VAMP algorithm are shown in **Algorithm 1**.

---

**Algorithm 1** Max-sum VAMP SVD

---

Given  $\mathbf{A} \in \mathbb{C}^{M \times N}$ ,  $\mathbf{z} \in \mathbb{C}^M$ , precision tolerance ( $\epsilon$ ) and maximum number of iterations ( $T_{\text{MAX}}$ )

```

1: Initialize  $\mathbf{r}_0$ ,  $\gamma_0 \geq 0$  and  $t \leftarrow 1$ 
2: Compute economy-size SVD  $\mathbf{A} = \mathbf{U}\text{Diag}(\boldsymbol{\omega})\mathbf{V}^H$ 
3:  $R_{\mathbf{A}} = \text{Rank}(\mathbf{A}) = \text{length}(\boldsymbol{\omega})$ 
4: Compute  $\tilde{\mathbf{z}} = \text{Diag}(\boldsymbol{\omega})^{-1}\mathbf{U}^H\mathbf{z}$ 
5: repeat
6:   // LMMSE SVD Form.
7:    $\mathbf{d}_t = \gamma_w \text{Diag}(\gamma_w \boldsymbol{\omega}^2 + \gamma_{t-1} \mathbf{1})^{-1} \boldsymbol{\omega}^2$ 
8:    $\tilde{\mathbf{r}}_t = \mathbf{r}_{t-1} + \frac{N}{R_{\mathbf{A}}} \mathbf{V} \text{Diag}(\mathbf{d}_t / \langle \mathbf{d}_t \rangle) (\tilde{\mathbf{z}} - \mathbf{V}^H \mathbf{r}_{t-1})$ 
9:    $\tilde{\gamma}_t = \gamma_{t-1} \langle \mathbf{d}_t \rangle / \left( \frac{N}{R_{\mathbf{A}}} - \langle \mathbf{d}_t \rangle \right)$ 
10:  // Denoiser
11:   $\hat{\mathbf{x}}_t = g_1(\tilde{\mathbf{r}}_t, \tilde{\gamma}_t)$ 
12:   $\hat{\gamma}_t = \langle g_1'(\tilde{\mathbf{r}}_t, \tilde{\gamma}_t) \rangle / \tilde{\gamma}_t$ 
13:   $\gamma_t = \hat{\gamma}_t - \tilde{\gamma}_t$ 
14:   $\mathbf{r}_t = (\hat{\gamma}_t \hat{\mathbf{x}}_t - \tilde{\gamma}_t \tilde{\mathbf{r}}_t) / \gamma_t$ 
15:   $t \leftarrow t + 1$ 
16: until  $\|\hat{\mathbf{x}}_t - \hat{\mathbf{x}}_{t-1}\|_2^2 \leq \epsilon \|\hat{\mathbf{x}}_{t-1}\|_2^2$  or  $t > T_{\text{MAX}}$ 
17: return  $\hat{\mathbf{x}}_t$ 

```

---

## B. VAMP for Optimization

In this section, we study how max-sum VAMP can be applied to constrained optimization problems. Given that we have matrices  $\mathbf{A} \in \mathbb{C}^{M \times N}$  and  $\mathbf{B} \in \mathbb{C}^{Q \times R}$ , the goal is to solve an

optimization problem of the form:

$$\arg \min_{\mathbf{X}} \|\mathbf{AXB} - \mathbf{Z}\|_F^2 \quad (20a)$$

$$\text{s.t. } f(x_{ik}) = 0, \quad (20b)$$

where  $\mathbf{X} \in \mathbb{C}^{N \times Q}$  with  $\mathbf{Z} \in \mathbb{C}^{M \times R}$ . In the context of optimization, the observation matrix,  $\mathbf{Z}$ , is considered as the desired output matrix and it is also assumed to be known. Unlike the estimation problem in (13), we do not have a prior distribution on  $\mathbf{X}$ . Yet the above optimization problem in (20) can be solved by modifying the modules of standard max-sum VAMP.

1) *Extended LMMSE*: Through vectorization, the objective function in (20) can be written in the same form of the objective function in (13) in the following way:

$$\text{vec}(\mathbf{Z}) = (\mathbf{B}^T \otimes \mathbf{A}) \text{vec}(\mathbf{X}). \quad (21)$$

The SVD form of VAMP allows for exploiting the Kronecker structure throughout the algorithm to avoid any large matrix multiplication. The product of a Kronecker matrix and a vector can be computed in an efficient way through reverse vectorization or *unvectorization* by computing the product of three smaller matrices, and then vectorizing the result. Let  $\mathbf{A} = \mathbf{U}_A \text{Diag}(\boldsymbol{\omega}_A) \mathbf{V}_A^H$ ,  $\mathbf{B}^T = \mathbf{U}_B \text{Diag}(\boldsymbol{\omega}_B) \mathbf{V}_B^H$  and  $(\mathbf{B}^T \otimes \mathbf{A}) = \mathbf{U} \text{Diag}(\boldsymbol{\omega}) \mathbf{V}^H$ . Using the fact that:

$$\mathbf{U} \text{Diag}(\boldsymbol{\omega}) \mathbf{V}^H = (\mathbf{U}_B \otimes \mathbf{U}_A) \text{Diag}(\boldsymbol{\omega}_B \otimes \boldsymbol{\omega}_A) (\mathbf{V}_B^H \otimes \mathbf{V}_A^H), \quad (22)$$

we modify the steps of **Algorithm 1** accordingly. Similar to the standard max-sum VAMP, at iteration  $t$ , the LMMSE module receives extrinsic mean matrix,  $\mathbf{R}_{t-1}$ , such that:  $\text{vec}(\mathbf{R}_{t-1}) = \mathbf{r}_{t-1}$ , and scalar variance  $\gamma_{t-1}^{-1}$  from the MAP estimator. First, the line 4 of the algorithm can be written as:

$$\begin{aligned} \tilde{\mathbf{Z}} &\triangleq \text{unvec}(\tilde{\mathbf{z}}) = \text{unvec}(\text{Diag}(\boldsymbol{\omega})^{-1} \mathbf{U}^H \text{vec}(\mathbf{Z})) \\ &= \text{Diag}(\boldsymbol{\omega}_A)^{-1} \mathbf{U}_A^H \mathbf{Z} (\text{Diag}(\boldsymbol{\omega}_B)^{-1} \mathbf{U}_B^H)^T. \end{aligned} \quad (23)$$

Similarly, the intermediary vector  $\mathbf{d}_t$  in line 7 of **Algorithm 1** can be re-expressed as follows:

$$\begin{aligned} \mathbf{d}_t &= \gamma_w \text{Diag}(\gamma_w (\boldsymbol{\omega}_B \otimes \boldsymbol{\omega}_A)^2 + \gamma_k \mathbf{1})^{-1} (\boldsymbol{\omega}_B \otimes \boldsymbol{\omega}_A)^2 \\ &= \gamma_w (\gamma_w (\boldsymbol{\omega}_B \otimes \boldsymbol{\omega}_A)^2 + \gamma_k \mathbf{1})^{-1} \odot (\boldsymbol{\omega}_B \otimes \boldsymbol{\omega}_A)^2. \end{aligned} \quad (24)$$

The extrinsic mean matrix,  $\tilde{\mathbf{R}}_t$ , and the scalar variance,  $\tilde{\gamma}_t^{-1}$ , are computed directly without needing to compute the LMMSE estimate,  $\bar{\mathbf{X}}_t$ , and posterior variance,  $\bar{\gamma}_t$ . While the step for

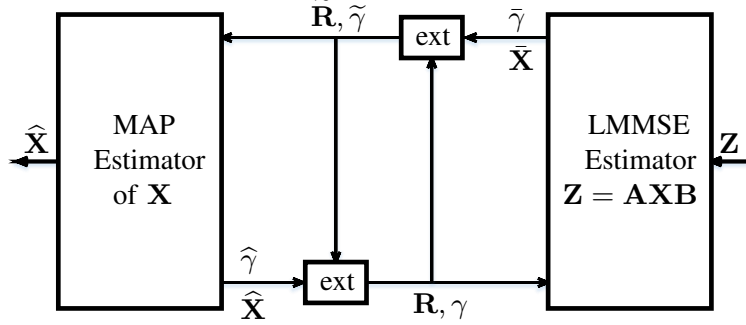


Fig. 2: Block diagram of batch VAMP for optimization.

computing extrinsic variance,  $\tilde{\gamma}_t^{-1}$ , remains unchanged, the extrinsic mean matrix,  $\tilde{\mathbf{R}}_t$ , is computed through unvectorization of the extrinsic mean vector,  $\tilde{\mathbf{r}}_t$ , as follows:

$$\begin{aligned} \tilde{\mathbf{R}}_t &= \text{unvec} \left( \mathbf{r}_{t-1} + \frac{NQ}{\text{Rank}(\mathbf{B} \otimes \mathbf{A})} \mathbf{V} \text{Diag} \left( \mathbf{d}_t / \langle \mathbf{d}_t \rangle \right) (\tilde{\mathbf{z}} - \mathbf{V}^H \mathbf{r}_{t-1}) \right) \\ &= \mathbf{R}_{t-1} + \frac{NQ}{\text{Rank}(\mathbf{B} \otimes \mathbf{A})} \mathbf{V}_A \left( \text{unvec} \left( \text{Diag} \left( \frac{\mathbf{d}_t}{\langle \mathbf{d}_t \rangle} \right) \text{vec} \left( \tilde{\mathbf{z}} - \mathbf{V}_A^H \mathbf{R}_{t-1} (\mathbf{V}_B^H)^T \right) \right) \right) \mathbf{V}_B^T. \end{aligned} \quad (25)$$

Hence, the only Kronecker product required for the LMMSE is of the two vectors  $\omega_B$  and  $\omega_A$ .

2) *Scalar MAP Estimator:* Because the constraint on  $\mathbf{X}$  is component-wise, we model the constraint on its entries,  $x_{ik}$ , as a prior with some precision,  $\gamma_p > 0$ , i.e.,  $p_x(x_{ik}) \propto \exp[-\gamma_p f(x_{ik})]$  and define the scalar denoiser function (now called projector function in the context of optimization) as follows:

$$\hat{x}_{ik,t} = g_{ik}(\tilde{r}_{ik,t}, \tilde{\gamma}_t) \triangleq \arg \min_{x_{ik}} [\tilde{\gamma}_t |r_{ik,t} - \tilde{r}_{ik,t}|^2 - \ln p_x(x_{ik})], \quad (26)$$

equivalently:

$$g_{ik}(\tilde{r}_{ik,t}, \tilde{\gamma}_t) = \arg \min_{x_{ik}} [\tilde{\gamma}_t |x_{ik} - \tilde{r}_{ik,t}|^2 + \gamma_p f(x_{ik})]. \quad (27)$$

The parameter  $\gamma_p$  in (27) governs weightage given to the constraint,  $f(x_{ik})$ . Choosing  $\gamma_p \gg \tilde{\gamma}$  enforces the constraint while choosing  $\gamma_p \ll \tilde{\gamma}$  ignores the constraint. Taking the derivative of the scalar projector function yields:

$$g'_{ik}(\tilde{r}_{ik,t}, \tilde{\gamma}_t) = \tilde{\gamma}_t \hat{\gamma}_t, \quad (28)$$

---

**Algorithm 2** Matrix max-sum VAMP SVD for optimization

---

Given  $\mathbf{A} \in \mathbb{C}^{M \times N}$ ,  $\mathbf{B} \in \mathbb{C}^{Q \times R}$ ,  $\mathbf{Z} \in \mathbb{C}^{M \times R}$ , precision tolerance ( $\epsilon$ ) and maximum number of iterations ( $T_{\text{MAX}}$ )

```

1: Select initial  $\mathbf{R}_0$ ,  $\gamma_0 \geq 0$  and  $t \leftarrow 1$ 
2: Compute economy-size SVD  $\mathbf{A} = \mathbf{U}_A \text{Diag}(\boldsymbol{\omega}_A) \mathbf{V}_A^H$ 
3: Compute economy-size SVD  $\mathbf{B}^T = \mathbf{U}_B \text{Diag}(\boldsymbol{\omega}_B) \mathbf{V}_B^H$ 
4: Compute  $\boldsymbol{\omega} = \boldsymbol{\omega}_B \otimes \boldsymbol{\omega}_A$ 
5:  $R_{B-A} = \text{Rank}(\mathbf{B}^T \otimes \mathbf{A}) = \text{length}(\boldsymbol{\omega})$ 
6: Compute  $\tilde{\mathbf{Z}} = \text{Diag}(\boldsymbol{\omega}_A)^{-1} \mathbf{U}_A^H \mathbf{Z} (\text{Diag}(\boldsymbol{\omega}_B)^{-1} \mathbf{U}_B^H)^T$ 
7: repeat
8:   // LMMSE SVD Form.
9:    $\mathbf{d}_t = \gamma_w (\gamma_w \boldsymbol{\omega}^2 + \gamma_{t-1} \mathbf{1})^{-1} \odot \boldsymbol{\omega}^2$ 
10:   $\hat{\mathbf{D}}_t = \text{unvec} \left( \frac{\mathbf{d}_t}{\langle \mathbf{d}_t \rangle} \odot \text{vec} \left( \tilde{\mathbf{Z}} - \mathbf{V}_A^H \mathbf{R}_{t-1} (\mathbf{V}_B^H)^T \right) \right)$ 
11:   $\tilde{\mathbf{R}}_t = \mathbf{R}_{t-1} + \frac{NQ}{R_{B-A}} \mathbf{V}_A \hat{\mathbf{D}}_t \mathbf{V}_B^T$ 
12:   $\tilde{\gamma}_t = \gamma_{t-1} \langle \mathbf{d}_t \rangle / \left( \frac{NQ}{R_{B-A}} - \langle \mathbf{d}_t \rangle \right)$ 
13:  // Projector.
14:   $\hat{\mathbf{X}}_t = g(\tilde{\mathbf{R}}_t, \tilde{\gamma})$ 
15:   $\hat{\gamma}_t = \langle g'(\tilde{\mathbf{R}}_t, \tilde{\gamma}) \rangle / \tilde{\gamma}_t$ 
16:   $\gamma_t = \hat{\gamma}_t - \tilde{\gamma}_t$ 
17:   $\mathbf{R}_t = (\hat{\gamma}_t \hat{\mathbf{X}}_t - \tilde{\gamma}_t \tilde{\mathbf{R}}_t) / \gamma_t$ 
18:   $t \leftarrow t + 1$ 
19: until  $\left\| \hat{\mathbf{X}}_t - \hat{\mathbf{X}}_{t-1} \right\|_F^2 \leq \epsilon \left\| \hat{\mathbf{X}}_{t-1} \right\|_F^2$  or  $t > T_{\text{MAX}}$ 
20: return  $\hat{\mathbf{X}}_t$ 

```

---

where  $\hat{\gamma}_t$  is the posterior precision. Similar to the denoiser module, extrinsic information from the projector module is calculated in the form of the mean matrix:

$$\begin{aligned}
\mathbf{R}_t &= \text{unvec} \left( \text{vec} \left( \hat{\mathbf{X}}_t \right) \hat{\gamma}_t - \text{vec} \left( \tilde{\mathbf{R}}_t \right) \tilde{\gamma}_t \right) / (\hat{\gamma}_t - \tilde{\gamma}_t) \\
&= \left( \hat{\mathbf{X}}_t \hat{\gamma}_t - \tilde{\mathbf{R}}_t \tilde{\gamma}_t \right) / (\hat{\gamma}_t - \tilde{\gamma}_t),
\end{aligned} \tag{29}$$

and scalar variance,  $\gamma_t^{-1} = (\hat{\gamma}_t - \tilde{\gamma}_t)^{-1}$  which are then fed to the LMMSE module. In an analogous way to sum-product VAMP, the max-sum VAMP (for optimization) decouples the

constraint from the objective function and also enables the projector function to be separable. The LMMSE module solves unconstrained optimization of the objective function, whereas the projector function enforces the constraint. This favorable property makes VAMP a robust algorithm for solving optimization problems in the presence of linear mixing and under various component-wise constraints. The complete steps for the VAMP for optimization are presented in **Algorithm 2**.

#### IV. VAMP-BASED SOLUTION FOR THE JOINT BEAMFORMING PROBLEM

In this section, we present a novel iterative algorithm that simultaneously finds optimal phase matrix,  $\Upsilon$ , as well as the optimal precoding matrix  $\mathbf{F}$ . We decouple the joint optimization problem into two sub-problems through alternate optimization. One of them finds the optimal phase matrix,  $\Upsilon$ , by utilizing the modified max-sum VAMP and the other sub-problem optimizes the transmit precoding  $\mathbf{F}$ .

##### A. Alternate Optimization

We use block coordinate descent to decompose the joint optimization problem into two simpler optimization problems. It is a simple iterative approach that optimizes one variable at a time<sup>1</sup> (while fixing the others) and the process is repeated for every variable. Thus, we divide the optimization problem in (8) into the following two sub-optimization problems:

1)

$$\arg \min_{\Upsilon} \mathbb{E}_{\mathbf{y}, \mathbf{s}} \left\{ \|\mathbf{y} - \mathbf{s}\|_2^2 \right\} \quad (30a)$$

$$\text{s.t. } v_{ik} = 0, \quad i \neq k \quad (30b)$$

$$|v_{ii}| = 0, \quad i = 1, 2, \dots, K. \quad (30c)$$

2)

$$\arg \min_{\alpha, \mathbf{F}} \mathbb{E}_{\mathbf{y}, \mathbf{s}} \left\{ \|\mathbf{y} - \mathbf{s}\|_2^2 \right\} \quad (31a)$$

$$\text{s.t. } \mathbb{E}_{\mathbf{s}} \|\mathbf{F}\mathbf{s}\|_2^2 = P. \quad (31b)$$

<sup>1</sup>Note here that a variable can be a scalar, a vector, or a whole matrix.

Let us define the error at iteration  $t$  as follows:

$$E(t) \triangleq \left\| \widehat{\alpha}_t \left( \mathbf{H}_{s-u}^H \widehat{\mathbf{\Upsilon}}_t \mathbf{H}_{b-s} + \mathbf{H}_{b-u}^H \right) \widehat{\mathbf{F}}_t - \mathbf{I}_M \right\|_F^2 + M \widehat{\alpha}_t^2 \sigma_w^2. \quad (32)$$

The algorithm stops iterating when  $|E(t) - E(t-1)| < \epsilon E(t-1)$ , where  $\epsilon \in \mathbb{R}_+$  is some precision tolerance. The algorithmic steps for BCD after taking expectation w.r.t  $\mathbf{s}$  and  $\mathbf{w}$  are shown in **Algorithm 3**.

---

**Algorithm 3** Block coordinate descent

---

Given  $\mathbf{H}_{s-u}$ ,  $\mathbf{H}_{b-u}$ ,  $\mathbf{H}_{b-s}$ , precision tolerance ( $\epsilon$ ), and maximum number of iterations ( $T_{MAX}$ )

- 1: Initialize  $\widehat{\mathbf{\Upsilon}}_0$  and  $t \leftarrow 1$ .
- 2: **repeat**
- 3: 
$$[\widehat{\alpha}_t, \widehat{\mathbf{F}}_t] = \arg \min_{\alpha, \mathbf{F}} \left\| \alpha \left( \mathbf{H}_{s-u}^H \widehat{\mathbf{\Upsilon}}_{t-1} \mathbf{H}_{b-s} + \mathbf{H}_{b-u}^H \right) \mathbf{F} - \mathbf{I}_M \right\|_F^2 + M \alpha^2 \sigma_w^2$$

$$\text{s.t. } \|\mathbf{F}\|_F^2 = P$$
- 4: 
$$\widehat{\mathbf{\Upsilon}}_t = \arg \min_{\mathbf{\Upsilon}} \left\| \widehat{\alpha}_t \left( \mathbf{H}_{s-u}^H \mathbf{\Upsilon} \mathbf{H}_{b-s} + \mathbf{H}_{b-u}^H \right) \widehat{\mathbf{F}}_t - \mathbf{I}_M \right\|_F^2$$

$$\text{s.t. } v_{ik} = 0 \quad i \neq k,$$

$$|v_{ii}| = 1 \quad i = 1, 2, \dots, K$$
- 5:  $t \leftarrow t + 1$
- 6: **until**  $|E(t) - E(t-1)| < \epsilon E(t-1)$  or  $t > T_{MAX}$
- 7: **return**  $\widehat{\mathbf{\Upsilon}}_t$ ,  $\widehat{\mathbf{F}}_t$ ,  $\widehat{\alpha}_t$ .

---

### B. Optimal Phase Matrix

We adapt max-sum VAMP in order to find the optimal phase matrix,  $\mathbf{\Upsilon}$ . Let us restate the associated optimization after taking expectation w.r.t.  $\mathbf{s}$  and  $\mathbf{w}$  in (30) as:

$$\arg \min_{\mathbf{\Upsilon}} \left\| \alpha \mathbf{H}_{s-u}^H \mathbf{\Upsilon} \mathbf{H}_{b-s} \mathbf{F} - (\mathbf{I}_M - \alpha \mathbf{H}_{b-u}^H \mathbf{F}) \right\|_F^2 \quad (33a)$$

$$\text{s.t. } v_{ik} = 0 \quad i \neq k, \quad (33b)$$

$$|v_{ii}| = 1 \quad i = 1, 2, \dots, K. \quad (33c)$$

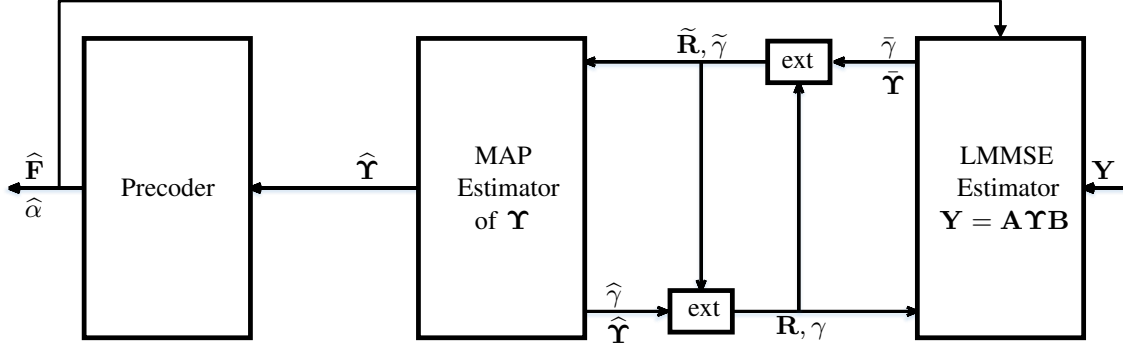


Fig. 3: Block diagram of the proposed algorithm.

The solution is obtained by setting  $\mathbf{A} = \alpha \mathbf{H}_{s-u}^H$ ,  $\mathbf{B} = \mathbf{H}_{b-s} \mathbf{F}$  and  $\mathbf{Z} = \mathbf{I}_M - \alpha \mathbf{H}_{b-u} \mathbf{F}$  in **Algorithm 2** and then choosing a suitable projector function to satisfy the constraints on reflection coefficients. The unconstrained minimization of the objective function in (33) is performed by the LMMSE module. We define the projector function that enforces the constraint on the reflection coefficients as:

$$g_{2,ik}(\tilde{r}_{ik}, \tilde{\gamma}) \triangleq \begin{cases} \arg \min_{v_{ik}} [\tilde{\gamma}|v_{ik} - \tilde{r}_{ik}|^2 - \gamma_p(|v_{ik}| - 1)^2] & i = k \\ 0 & i \neq k. \end{cases} \quad (34)$$

Solving the optimization problem in (34) for  $i = k$  results in the following closed-form expression for the underlying projector function

$$g_{2,ii}(\tilde{r}_{ii}, \tilde{\gamma}) = \frac{\tilde{\gamma}}{\tilde{\gamma} + \gamma_p} \tilde{r}_{ii} + \frac{\gamma_p}{\tilde{\gamma} + \gamma_p} \tilde{r}_{ii} |\tilde{r}_{ii}|^{-1}. \quad (35)$$

To enforce the constraint, we choose  $\gamma_p \gg \tilde{\gamma}$  such that  $\frac{\tilde{\gamma}}{\tilde{\gamma} + \gamma_p} \approx 0$  and  $\frac{\gamma_p}{\tilde{\gamma} + \gamma_p} \approx 1$ . Therefore, the projector function simplifies to:

$$g_{2,ik}(\tilde{r}_{ik}) = \begin{cases} \tilde{r}_{ik} |\tilde{r}_{ik}|^{-1} & i = k \\ 0 & i \neq k. \end{cases} \quad (36)$$

Finally, the derivative of the projector function (36) w.r.t.  $\tilde{r}_{ik}$  is obtained as follows:

$$g'_{2,ik}(\tilde{r}_{ik}) = \begin{cases} \frac{1}{2} |\tilde{r}_{ik}|^{-1} & i = k \\ 0 & i \neq k. \end{cases} \quad (37)$$

### C. Optimal Precoding

The sub-optimization problem in (31) is a constrained MMSE transmit precoding optimization for a MIMO system. It can be solved by jointly optimizing  $\mathbf{F}$  and  $\alpha$  using Lagrange optimization. We construct the Lagrangian function for the problem (31) after taking expectation as follows:

$$\mathcal{L}(\mathbf{F}, \alpha, \lambda) = \left\| \alpha \mathbf{H}^H \mathbf{F} - \mathbf{I}_M \right\|_F^2 + M\alpha^2 \sigma_w^2 + \lambda(\text{Tr}(\mathbf{F}\mathbf{F}^H) - P), \quad (38)$$

with  $\lambda \in \mathbb{R}$  being the Lagrange multiplier. The closed-form solutions for optimal  $\alpha$  and  $\mathbf{F}$  are given below and we refer the reader to [28] for more details:

$$\alpha^{\text{opt}} = g_3(\mathbf{H}) \triangleq \sqrt{\frac{1}{P}} \sqrt{\text{Tr} \left( \left[ \mathbf{H} \mathbf{H}^H + \frac{M\sigma_w^2 \mathbf{I}_N}{P} \right]^{-2} \mathbf{H} \mathbf{H}^H \right)}. \quad (39)$$

$$\mathbf{F}^{\text{opt}} = g_4(\mathbf{H}) \triangleq \frac{\sqrt{P} \left[ \mathbf{H} \mathbf{H}^H + \frac{M\sigma_w^2 \mathbf{I}_N}{P} \right]^{-1} \mathbf{H}}{\sqrt{\text{Tr} \left( \left[ \mathbf{H} \mathbf{H}^H + \frac{M\sigma_w^2 \mathbf{I}_N}{P} \right]^{-2} \mathbf{H} \mathbf{H}^H \right)}}. \quad (40)$$

It is worth mentioning here that, on the receiver side,  $\alpha$  can be obtained in a blind manner based on the received signal power as it is just a scalar and independent of the transmitted signal. Consequently, the receiver does not require any additional information from the BS (e.g., the phase matrix  $\mathbf{\Upsilon}$ ) to calculate  $\alpha$ .

Now that we have solved both sub-optimization problems required for the coordinate descent algorithm (i.e., **Algorithm 3**). We substitute the solutions to the sub-optimization problems in (30) and in (31) into **Algorithm 3**. The overall steps are stated in **Algorithm 4**.

## V. JOINT BEAMFORMING UNDER REACTIVE LOADING AT THE IRS

We consider a reflective element that is combined with a tunable reactive load instead of an ideal phase shifter, i.e., <sup>2</sup>  $v_{ii} = (1 + j\chi_{ii})^{-1}$  where  $\chi_{ii} \in \mathbb{R}$  is a scalar reactance value that has

<sup>2</sup>The value 1 is the normalized resistive part of the element impedance whereas  $\chi_{ii}$  is the normalized reactive part of the antenna plus reactive termination. Accordingly  $v_{ii}$  represents the induced current flowing across the antenna. We assume the antenna elements to be uncoupled which holds approximately for half-wavelength element spacing.

---

**Algorithm 4** VAMP-based joint optimization algorithm

---

Given  $\mathbf{H}_{s-u}$ ,  $\mathbf{H}_{b-u}$ ,  $\mathbf{H}_{b-s}$ , precision tolerance ( $\epsilon$ ), and maximum number of iterations ( $T_{MAX}$ )

- 1: Initialize  $\widehat{\mathbf{Y}}_0$ ,  $\mathbf{R}_0$ ,  $\gamma_0 \geq 0$  and  $t \leftarrow 1$
- 2:  $\widehat{\mathbf{H}}_0 = \left( \mathbf{H}_{s-u}^H \widehat{\mathbf{Y}}_0 \mathbf{H}_{b-s} + \mathbf{H}_{b-u}^H \right)^H$
- 3:  $\widehat{\alpha}_0 = g_3 \left( \widehat{\mathbf{H}}_0 \right)$
- 4:  $\widehat{\mathbf{F}}_0 = g_4 \left( \widehat{\mathbf{H}}_0 \right)$
- 5: **repeat**
- 6:   // LMMSE SVD Form.
- 7:    $\mathbf{A} = \alpha_{t-1} \mathbf{H}_{s-u}^H$
- 8:    $\mathbf{B} = \mathbf{H}_{b-s} \mathbf{F}_{t-1}.$
- 9:    $\mathbf{Y} = \mathbf{I}_M - \alpha_{t-1} \mathbf{H}_{b-u}^H \mathbf{F}_{t-1}$
- 10:   Compute economy-size SVD  $\mathbf{A} = \mathbf{U}_A \text{Diag}(\boldsymbol{\omega}_A) \mathbf{V}_A^H$
- 11:   Compute economy-size SVD  $\mathbf{B}^T = \mathbf{U}_B \text{Diag}(\boldsymbol{\omega}_B) \mathbf{V}_B^H$
- 12:   Compute  $\boldsymbol{\omega} = \boldsymbol{\omega}_B \otimes \boldsymbol{\omega}_A$
- 13:    $R_{B-A} = \text{Rank}(\mathbf{B}^T \otimes \mathbf{A}) = \text{length}(\boldsymbol{\omega})$
- 14:   Compute  $\widetilde{\mathbf{Y}} =: \text{Diag}(\boldsymbol{\omega}_A)^{-1} \mathbf{U}_A^H \mathbf{Y} \left( \text{Diag}(\boldsymbol{\omega}_B)^{-1} \mathbf{U}_B^H \right)^T$
- 15:    $\mathbf{d}_t = \gamma_w (\gamma_w \boldsymbol{\omega}^2 + \gamma_{t-1} \mathbf{1})^{-1} \odot \boldsymbol{\omega}^2$
- 16:    $\widehat{\mathbf{D}}_t = \text{unvec} \left( \frac{\mathbf{d}_t}{\langle \mathbf{d}_t \rangle} \odot \text{vec} \left( \widetilde{\mathbf{Y}} - \mathbf{V}_A^H \mathbf{R}_{t-1} \left( \mathbf{V}_B^H \right)^T \right) \right)$
- 17:    $\widetilde{\mathbf{R}}_t = \mathbf{R}_{t-1} + \frac{K^2}{R_{B-A}} \mathbf{V}_A \widehat{\mathbf{D}}_t \mathbf{V}_B^T$
- 18:    $\widetilde{\gamma}_t = \gamma_{t-1} \langle \mathbf{d}_t \rangle / \left( \frac{K^2}{R_{B-A}} - \langle \mathbf{d}_t \rangle \right)$
- 19:   // Projector Part
- 20:    $\widehat{\mathbf{Y}}_t = g_2 \left( \widetilde{\mathbf{R}}_t \right)$
- 21:    $\widehat{\gamma}_t = \left\langle g'_2 \left( \widetilde{\mathbf{R}}_t \right) \right\rangle / \widetilde{\gamma}_t.$
- 22:    $\gamma_t = \widehat{\gamma}_t - \widetilde{\gamma}_t$
- 23:    $\mathbf{R}_t = \left( \widehat{\gamma}_t \widehat{\mathbf{Y}}_t - \widetilde{\gamma}_t \widetilde{\mathbf{R}}_t \right) / \gamma_t$
- 24:   //Find  $\alpha$  and  $\mathbf{F}$  through their closed-form solutions.
- 25:    $\widehat{\mathbf{H}}_t = \left( \mathbf{H}_{s-u}^H \widehat{\mathbf{Y}}_t \mathbf{H}_{b-s} + \mathbf{H}_{b-u}^H \right)^H$
- 26:    $\widehat{\alpha}_t = g_3 \left( \widehat{\mathbf{H}}_t \right)$
- 27:    $\widehat{\mathbf{F}}_t = g_4 \left( \widehat{\mathbf{H}}_t \right)$
- 28:    $t \leftarrow t + 1$
- 29: **until**  $|E(t) - E(t-1)| < \epsilon E(t-1)$  or  $t > T_{MAX}$
- 30: **return**  $\widehat{\mathbf{Y}}_t$ ,  $\widehat{\mathbf{F}}_t$ ,  $\widehat{\alpha}_t$ .

---

to be optimized for each reflection coefficient. We rewrite the objective function under the new constraint on phases as follows:

$$\arg \min_{\mathbf{Y}} \left\| \alpha \mathbf{H}_{s-u}^H \mathbf{Y} \mathbf{H}_{b-s} \mathbf{F} - (\mathbf{I}_M - \alpha \mathbf{H}_{b-u}^H \mathbf{F}) \right\|_F^2 \quad (41a)$$

$$\text{s.t. } v_{ik} = 0, \quad i \neq k, \quad (41b)$$

$$v_{ii} = \frac{1}{1 + j\chi_{ii}}, \quad i = 1, 2, \dots, K. \quad (41c)$$

To find the optimal phase matrix under the new constraint, we change the projector function accordingly as follows:

$$g_{5,ik}(\tilde{r}_{ik}, \tilde{\gamma}) \triangleq \begin{cases} \arg \min_{v_{ik}} \left[ \tilde{\gamma} |v_{ik} - \tilde{r}_{ik}|^2 + \gamma_p \left( v_{ik} - \frac{1}{1 + j\chi_{ii}^{\text{opt}}} \right)^2 \right] & i = k \\ 0 & i \neq k, \end{cases} \quad (42)$$

where

$$\chi_{ii}^{\text{opt}} = g_6(\tilde{r}_{ii}) \triangleq \arg \min_{\chi_{ii}} \left| \tilde{r}_{ii} - \frac{1}{1 + j\chi_{ii}} \right|^2. \quad (43)$$

The optimization problem in (42) is a bi-level one [29]. The solution to (43) is substituted in (42) and then solved as ordinary MAP optimization. We show in **Appendix A** that the solution to (43) is given by:

$$g_6(\tilde{r}_{ii}) = \frac{1}{2\Im\{\tilde{r}_{ii}\}} \left( 2\Re\{\tilde{r}_{ii}\} - 1 - \sqrt{(1 - 2\Re\{\tilde{r}_{ii}\})^2 + 4\Im\{\tilde{r}_{ii}\}^2} \right). \quad (44)$$

Substituting (44) back into (42) and solving the minimization leads to the following result:

$$g_{5,ii}(\tilde{r}_{ii}, \tilde{\gamma}) = \frac{\tilde{\gamma}}{\tilde{\gamma} + \gamma_p} \tilde{r}_{ii} + \frac{\gamma_p}{\tilde{\gamma} + \gamma_p} (1 + jg_6(\tilde{r}_{ii}))^{-1}. \quad (45)$$

The parameter  $\gamma_p$  is chosen in the same way as in Section IV-B to ensure that the constraint is satisfied. Thus, the projector function can be expressed as:

$$g_{5,ik}(\tilde{r}_{ik}) = \begin{cases} (1 + jg_6(\tilde{r}_{ik}))^{-1} & i = k \\ 0 & i \neq k, \end{cases} \quad (46)$$

whose derivative is obtained as follows:

$$g'_{5,ik}(\tilde{r}_{ik}) = \begin{cases} -jg'_6(\tilde{r}_{ik}) (1 + jg_6(\tilde{r}_{ik}))^{-2} & i = k \\ 0 & i \neq k, \end{cases} \quad (47)$$

where

$$g'_6(\tilde{r}_{ii}) = \frac{1}{2} \left( \frac{\partial g_6(\tilde{r}_{ii})}{\partial \Re\{\tilde{r}_{ii}\}} - j \frac{\partial g_6(\tilde{r}_{ii})}{\partial \Im\{\tilde{r}_{ii}\}} \right). \quad (48)$$

The partial derivatives involved in (48) are given by:

$$\frac{\partial g_6(\tilde{r}_{ii})}{\partial \Re\{\tilde{r}_{ii}\}} = \Im\{\tilde{r}_{ii}\}^{-1} + (1 - 2\Re\{\tilde{r}_{ii}\}) \left( \Im\{\tilde{r}_{ii}\} \sqrt{(1 - 2\Re\{\tilde{r}_{ii}\})^2 + 4\Im\{\tilde{r}_{ii}\}^2} \right)^{-1}, \quad (49)$$

and

$$\begin{aligned} \frac{\partial g_6(\tilde{r}_{ii})}{\partial \Im\{\tilde{r}_{ii}\}} &= (1 - 2\Re\{\tilde{r}_{ii}\}) (2\Im\{\tilde{r}_{ii}\})^{-1} \\ &+ (1 - 2\Re\{\tilde{r}_{ii}\})^2 \left( 2\Im\{\tilde{r}_{ii}\}^2 \sqrt{(1 - 2\Re\{\tilde{r}_{ii}\})^2 + 4\Im\{\tilde{r}_{ii}\}^2} \right)^{-1}. \end{aligned} \quad (50)$$

Since the derivative is required to be a real scalar, we take the absolute value of the complex derivative and, therefore, we modify the derivative of the projector function (47) as follows:

$$g'_{5,ik}(\tilde{r}_{ik}) = \begin{cases} |-jg'_6(\tilde{r}_{ii})(1+jg_6(\tilde{r}_{ii}))^{-2}| & i = k \\ 0 & i \neq k. \end{cases} \quad (51)$$

Lastly, we replace the projector function,  $g_2$ , with  $g_5$  in lines 19 and 20 of **Algorithm 4**.

## VI. NUMERICAL RESULTS: PERFORMANCE AND COMPLEXITY ANALYSIS

### A. Simulation Model and Parameters

We present simulation results to assess the performance of the proposed algorithm. We assume that the IRS is located at a fixed distance of 150 m from the BS and the users are spread uniformly at a radial distance of 20 m to 50 m from the IRS. A path-based propagation channel model, also known as parametric channel model [22], is used. Such model accounts for both scattered and reflected signal components. The channel between the IRS and the BS is generated according

TABLE I: Simulation parameters and their notations

Parameter	Notation	Parameter	Notation
IRS antenna spacing	$d_s$	BS antenna spacing	$d_b$
Angle of departure (BS array vector)	$\phi$	Elevation angle (IRS array vector)	$\varphi$
Azimuth angle (IRS array vector)	$\psi$	Channel path gain	$c$
IRS-BS distance	$d_{\text{IRS}}$	User-IRS distance	$d$
User-BS distance	$d'$	Path-loss at reference distance	$C_0$
Reference distance	$d_0$	Path-loss exponent	$\eta$
Number of channel paths	$Q$	Noise variance	$\sigma_w^2$

to:

$$\mathbf{H}_{b-s} = \sqrt{L(d_{IRS})} \sum_{q=1}^{Q_{IRS}} c_q \mathbf{a}_{IRS}(\varphi_q, \psi_q) \mathbf{a}_{BS}(\phi_q)^T. \quad (52)$$

Here,  $Q_{IRS}$  and  $L(d_{IRS})$  denote the number of channel paths and the distance-dependent path-loss factor, respectively. The vectors  $\mathbf{a}_{BS}(\phi)$  and  $\mathbf{a}_{IRS}(\varphi, \psi)$  are array response vectors for the BS and the IRS, respectively. The coefficients  $c_q$  in (52) denote the path gains which are modeled by a complex normal distribution  $c_q \sim \mathcal{CN}(c_q; 0, 1)$ . Assuming uniform linear array (ULA) with  $N$  antennas is used at the BS, we have  $\mathbf{a}_{BS}(\phi) = [1, e^{2\pi j \frac{d_b}{\lambda} \cos \phi}, \dots, e^{2\pi j \frac{d_b}{\lambda} (N-1) \cos \phi}]^T$  wherein  $\lambda$ ,  $\phi$  and  $d_b$  represent wavelength, angle of departure (AOD), and inter-antenna spacing at the BS, respectively. The IRS is equipped with (square) uniform planar array (UPA) with  $K$  antenna elements. The array response vector for the IRS is expressed as follows:

$$\mathbf{a}_{IRS}(\varphi, \psi) = \sqrt{|\cos \varphi|} \begin{bmatrix} 1 \\ e^{2\pi j \frac{d_s}{\lambda} \sin \varphi \sin \psi} \\ \vdots \\ e^{2\pi j \frac{d_s}{\lambda} (\sqrt{K}-1) \sin \varphi \sin \psi} \end{bmatrix} \otimes \begin{bmatrix} 1 \\ e^{2\pi j \frac{d_s}{\lambda} \sin \varphi \cos \psi} \\ \vdots \\ e^{2\pi j \frac{d_s}{\lambda} (\sqrt{K}-1) \sin \varphi \cos \psi} \end{bmatrix}, \quad (53)$$

Here  $d_s$  represents inter-antenna spacing at the IRS whereas  $\varphi$  and  $\psi$  are angles of elevation and azimuth, respectively. In simulations we set  $d_b = d_s = \lambda/2$ . All three angles  $\phi$ ,  $\varphi$  and  $\psi$  are uniformly distributed in the interval  $[0, 2\pi)$ . The channel of direct link between the BS and the single-antenna user  $m$  with  $Q_{b-u}$  number of paths is modeled as follows:

$$\mathbf{h}_{b-u,m} = \sqrt{L(d_m)} \sum_{q=1}^{Q_{b-u}} c_{m,q} \mathbf{a}_{BS}(\phi_{m,q}), \quad m = 1, \dots, M. \quad (54)$$

Similar to the IRS-BS channel,  $c_{m,q} \sim \mathcal{CN}(c_{m,q}; 0, 1)$  and the angle  $\phi_m$  is uniformly distributed in  $[0, 2\pi)$ . The channel vectors in (54) are assumed to be independent among users. Finally, the channel vector for the link between each  $m$ -th user and the IRS with  $Q_{s-u}$  channel paths is modeled as follows:

$$\mathbf{h}_{s-u,m} = \sqrt{L(d'_m)} \sum_{q=1}^{Q_{s-u}} c_{m,q} \mathbf{a}_{IRS}(\varphi_{m,q}, \psi_{m,q}). \quad (55)$$

The term  $L(d) = C_0(d/d_0)^\eta$  in (52), (54), (55) is the distance-dependent path-loss factor, where  $C_0$  denotes the path-loss at a reference distance  $d_0 = 1$  m, and  $\eta$  is the path-loss exponent. Moreover, to include the line-of-sight (LOS) component in the channel, the gain of one channel path is set to a minimum of 5 dB higher than the other channel paths. In the simulations, for the IRS-BS channel,  $d_{IRS} = 150$  m is fixed whereas the user-BS distance,  $d$ , and user-IRS

distance,  $d'$ , vary for each user according to its location from the BS and the IRS, respectively. In all simulations, we set  $C_0 = -30$  dB,  $\eta = 3.7$  (NLOS channel),  $\eta = 2$  (LOS channel),  $Q_{b-u} = 2$ ,  $Q_{s-u} = 2$ ,  $Q_{IRS} = 10$ ,  $\epsilon = 10^{-4}$  and  $\sigma_w^2 = 1$ . The results are averaged over 1000 channel realizations.

We consider the following two scenarios: First, we consider a case where none of the channels contains a LOS component. Then we consider the case scenario where BS-IRS and IRS-user channels have a LOS component but all the direct BS-user channels have no LOS component. The proposed VAMP-base algorithm is compared against the following three different configurations:

- i. A MIMO system assisted by one IRS where the joint optimization of the phase matrix the and precoding is solved through alternate optimization and penalty-based ADMM.
- ii. A massive MIMO system with a large number of BS antennas where optimal precoding is computed using the maximal ratio transmission (MRT) technique.
- iii. An IRS-assisted MIMO system with unoptimized IRS phases and MMSE transmit precoding.

### B. Benchmarking Metrics

We use the two metrics for performance evaluation, namely the *sum-rate*,  $\widehat{C}$ , and the *normalized root mean square error* (NRMSE) which are defined as follows:

$$\widehat{C} = \sum_{m=1}^M \log_2 (1 + \rho_m), \quad (56)$$

where SINR,  $\rho_m$ , of user  $m$  is given by:

$$\rho_m = \frac{|\mathbf{h}_m^H \mathbf{f}_m|^2}{\sigma_w^2 + \sum_{i \neq m} |\mathbf{h}_m^H \mathbf{f}_i|^2}, \quad (57)$$

where  $\mathbf{h}_m^H = \mathbf{h}_{s-u,m}^H \boldsymbol{\Upsilon} \mathbf{H}_{b-s} + \mathbf{h}_{b-u,m}^H$ .

$$\text{NRMSE}(\alpha, \boldsymbol{\Upsilon}, \mathbf{F}) \triangleq \frac{1}{\sqrt{M}} \sqrt{\left\| \alpha (\mathbf{H}_{s-u}^H \boldsymbol{\Upsilon} \mathbf{H}_{b-s} + \mathbf{H}_{b-u}^H) \mathbf{F} - \mathbf{I}_M \right\|_F^2 + M \alpha^2 \sigma_w^2}, \quad (58)$$

### C. Performance Results

1) *NLOS Scenario*: Here we set the number of users to  $M = 9$  and the number of BS antennas to  $N = 32$  for every configuration except for massive MIMO for which we use  $N = 512$ . Fig. 4(a), depicts the achievable sum rate versus the transmit power,  $P$ , for the different

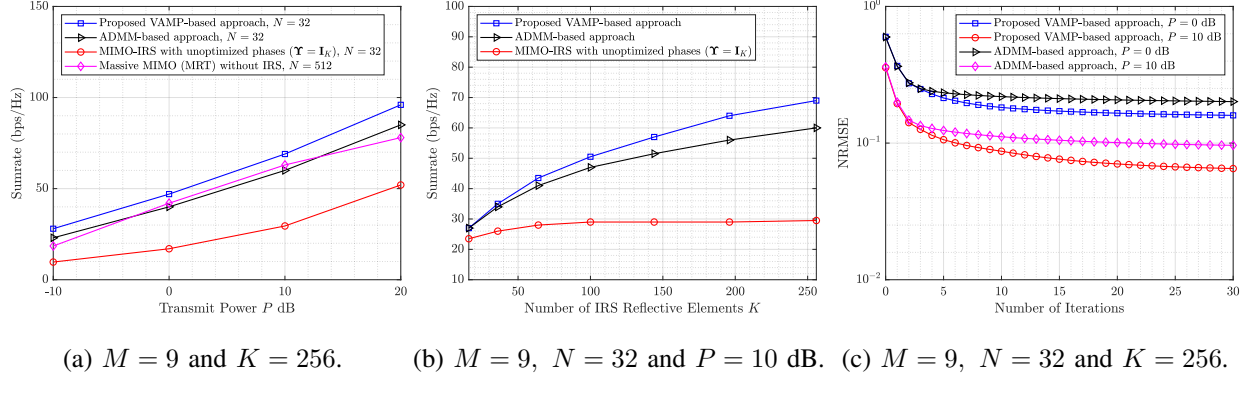
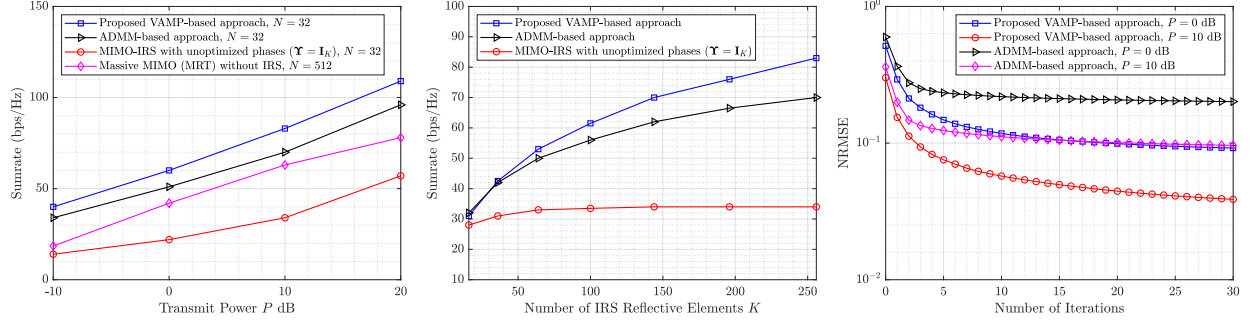


Fig. 4: NLOS channels: (a) Sum-rate versus transmit power, (b) Sum-rate versus the number of IRS reflective elements, and (c) NRMSE versus the number of iterations.

considered transmission schemes. The superiority of the proposed algorithm can be observed as it outperforms massive MIMO system with a significantly smaller number of transmit antennas. Since the proposed algorithm is based on VAMP, it outperforms the ADMM based solution due to the automatic tuning of scalar parameters (i.e., scalar precisions) by VAMP which behave similarly to a penalty parameter inside the algorithm. This improves convergence, unlike ADMM, where the penalty parameter must be manually chosen. As per the IRS-assisted configuration, where we do not optimize the reflection coefficients (i.e.,  $\Upsilon = \mathbf{I}_K$ ), a huge gap is observed between the achieved sum-rates as compared to the proposed algorithm.

Fig. 4(b) shows a plot of sum-rate against the number of IRS reflective elements. It is to be observed that even with a small number of active transmitting antennas and merely ten paths between the IRS and the BS, the sum-rate for the proposed solution keeps increasing with the increasing number of reflective elements. In contrast, the sum-rate saturates after a small gain when the IRS reflection coefficients are not optimized. Compared to ADMM, the proposed algorithm shows higher throughput at every point.

The convergence of the proposed algorithm is investigated in Fig. 4(c) which depicts the NRMSE as a function of the number of iterations. Observe that the major portion of the gain is achieved in the first few iterations. The small number of iterations required for convergence in combination with the low per-iteration complexity makes the proposed algorithm very attractive from the practical implementation point of view. The superiority of the proposed VAMP-based algorithm over the ADMM-based approach because of the feedback mechanism of VAMP that



(a)  $M = 9$  and  $K = 256$ . (b)  $M = 9$ ,  $N = 32$  and  $P = 10$  dB. (c)  $M = 9$ ,  $N = 32$  and  $K = 256$ .

Fig. 5: LOS IRS-user, BS-IRS channels: (a) Sum-rate versus transmit power, (b) Sum-rate versus the number of IRS reflection elements, and (c) NRMSE versus the number of iterations.

controls the weightage given to the  $\Upsilon$  computed in each iteration compared to that of the preceding iteration with the help of scalar precision parameters that act as weighting coefficients for  $\Upsilon$  computed in the current and the preceding iteration. In addition to the plots shifting downward, the increase in transmit power widens the gap between ADMM and the proposed VAMP-based algorithm. This demonstrates that the proposed algorithm utilizes the available transmit power in a more efficient way than ADMM.

2) *BS-IRS and IRS-user Channels with LOS components*: This situation is encountered in typical urban/suburban environments where the BS is located far away from the users and has no direct LOS component. However, the IRS is installed at a location where a LOS component is present in the BS-IRS link as well as the user-IRS link. We include a LOS path in the IRS-BS channel and in the user-IRS channels by setting the gain of one path 6 dB higher than the others.

Fig. 5(a) illustrates the sum-rate versus the transmit power for this configuration. As expected, the results show that by adding the LOS component, the use of an IRS together with the proposed joint beamforming optimization solution yields considerably higher sum-rates compared to a massive MIMO system with no IRS. Moreover, although the ADMM-based solution now outperforms massive MIMO, the advantage of the proposed VAMP-based solution over ADMM is higher when compared to the NLOS channels.

The results in Fig. 5(b), i.e., sum-rate vs the number of IRS reflective elements, also exhibit the same trends as in the NLOS channel yet with a broader gap between the plots, thereby, corroborating the superiority of the proposed solution. This is because the presence of a LOS component

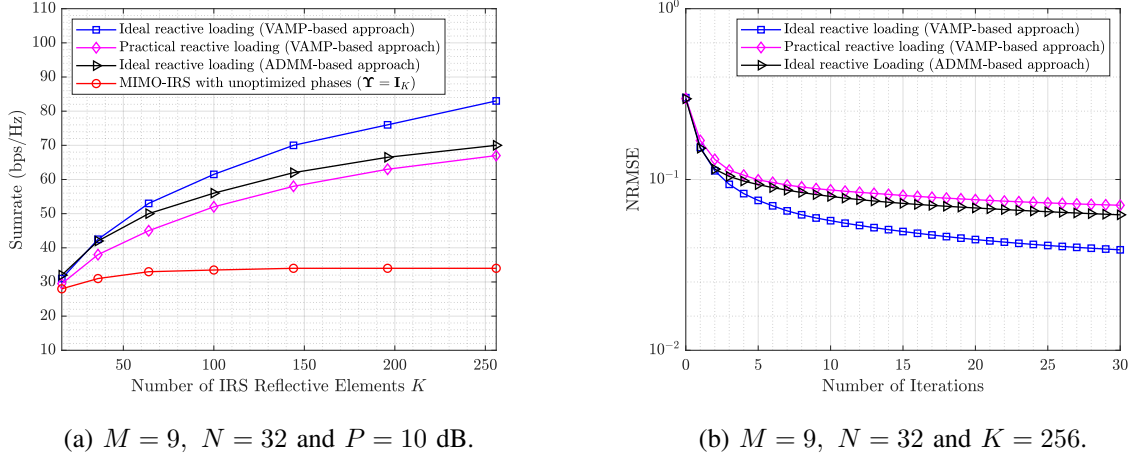


Fig. 6: LOS IRS-user, BS-IRS channels: (a) Sum-rate versus IRS elements with simple reactive loading, and (b) NRMSE versus the number of iterations.

helps the VAMP-based joint beamforming scheme to focus most of the transmit/reflected energy in that direction. This is clearly depicted in Fig. 5(c), where the NRMSE achieved by the proposed algorithm is approximately equivalent to the NRMSE achieved by the ADMM-based solution but at almost 10 dB lower SNR.

3) *Reactive Loading at the IRS*: In this subsection, we assess the effect of replacing the unimodular constraint on the reflection coefficients by a reactive load. We use the same channel configuration in Section VI-C2. But, we rely on optimizing just the reactive part of the reflection coefficients. Therefore, as portrayed by Fig. 6(a), the new constraint decreases the throughput when compared with ideal phase shifters setup. However, the resulting sum-rate is still much higher than the one obtained by using unoptimized IRS reflection coefficients. Similarly, due to having less room for optimizing the optimal reflection coefficients, Fig. 6(b) shows that the NRMSE saturates sooner and at a higher value as compared to the case of a unimodular constraint. Nonetheless, even with the more practical reactive load constraint, the resulting NRMSE is close to the NRMSE achieved by the ADMM with ideal phase shifters.

#### D. Complexity Analysis and CPU Execution Time

Note that, by utilizing the Kronecker structure, we successfully avoid any large matrix multiplication or even taking SVD of Kronecker products of matrices. Indeed, let  $\mathbf{A} = \alpha \mathbf{H}_{s-u}^H$  and  $\mathbf{B} = \mathbf{H}_{b-u} \mathbf{F}$ . For our system model, the matrices  $\mathbf{A}$  and  $\mathbf{B}^T$  are of the same size  $M \times K$ .

TABLE II: (a) Comparison between CPU execution time of the proposed VAMP-based algorithm and the ADMM-based algorithm for various design configurations, and (b) CPU running time for a fixed number of iterations for different design configurations.

II(a) Algorithm terminates when  $\text{NRMSE} < 10^{-1}$  or  $t > 100$ .

Design Parameters	VAMP-based algorithm (msec)	ADMM-based algorithm (msec)
$M = 2, N = 16, K = 64$	1.3	1.4
$M = 8, N = 16, K = 64$	45	53
$M = 2, N = 16, K = 256$	6.5	6.5
$M = 8, N = 16, K = 256$	47	85

II(b) Algorithm terminates when  $t > 30$ .

Design Parameters	VAMP-based algorithm (msec)
$M = 4, N = 64, K = 64$	31.5
$M = 8, N = 64, K = 64$	35
$M = 4, N = 64, K = 256$	117
$M = 8, N = 64, K = 256$	125
$M = 4, N = 256, K = 64$	410
$M = 8, N = 256, K = 64$	424

Assuming that the matrices  $\mathbf{A}$  and  $\mathbf{B}$  to be full rank, the complexity of the truncated SVDs of the matrices is in the order of  $\mathcal{O}(M^2K)$ . The computational complexity of the Kronecker product of two vectors in line 12 of **Algorithm 4** is in the order of  $\mathcal{O}(M^2)$ . The component-wise products of vectors in lines 15 and 16 are also of order  $\mathcal{O}(M^2)$ . The projector function and its derivative has a complexity order of  $\mathcal{O}(K)$ . The functions  $g_3(\mathbf{H})$  and  $g_4(\mathbf{H})$  entail a complexity of  $\mathcal{O}(MN^2 + N^3)$ . The complexity of all other matrix multiplication operations elsewhere including the LMMSE part are dominated by  $\mathcal{O}(MNK + MK^2)$ . Therefore, the overall per iteration complexity of the algorithm is of order  $\mathcal{O}(M^2K + MNK + MK^2 + MN^2 + N^3)$ . Since  $M < N$  in our case, the overall per iteration complexity simplifies to  $\mathcal{O}(MNK + MK^2 + N^3)$ . Table II(a) provides a comparison of CPU (central processing unit) utilization time between the VAMP-based solution and the ADMM-based approach for different design configurations. For

comparison purpose, we measure the time until the NRMSE falls below a certain value, therefore we run the algorithms until  $\text{NRMSE} < 10^{-1}$  or  $t > T_{\text{MAX}}$  while setting  $T_{\text{MAX}} = 100$ . We set the channel simulation parameters as in Section VI-C2 with  $P = 10$  dB. The algorithms are simulated on MATLAB R2020a on a laptop PC having a Core i7-4720HQ processor and 16 GB of RAM with Windows 10 operating system. The superiority of the proposed solution over the ADMM-based approach in terms of convergence time is especially highlighted in the case when there is a high number of users to serve, which requires efficient utilization of the IRS reflection elements in order to achieve the desired NRMSE. To validate the theoretical complexity of the VAMP-based solution, we run the proposed algorithm for a fixed number of iterations by setting  $T_{\text{MAX}} = 30$  for different design configurations. It is seen from Table II(b) that the numerical results of the proposed solution coincide with the aforementioned complexity analysis. In other words, the results are in line with the fact that the complexity is cubic in  $N$ , quadratic in  $K$ , and only linear in  $M$ .

## VII. CONCLUSION

We tackled the problem of joint active and passive beamforming design for an IRS-assisted downlink multi-user MIMO system. Using block coordinate descent, overall optimization was decomposed into two sub-optimization tasks. We presented a novel approach of utilizing the approximate message passing-based low-complexity VAMP algorithm to solve the optimization problem at hand. We did so by first extending the traditional VAMP algorithm and then used the extended version to find the optimal phase shifters matrix that must be used by the IRS. The optimal precoder at the BS, however, was found in closed-form using Lagrange optimization. The overall algorithm was shown to have low per-iteration complexity, which is quadratic with the number of IRS reflective elements, cubic with the number of BS antennas, but grows only linearly with the number of users. We also devised a more practical version of the proposed design by solving the joint optimization problem under a different constraint on the reflection coefficients, wherein each antenna element is terminated by a reactive load instead of an ideal phase shifter. Numerical results suggest that, with a small number of active BS antennas, the proposed solution yields higher throughput or spectral efficiency than a massive MIMO system under both LOS and NLOS propagation conditions. We also gauged the convergence of the proposed solution against ADMM and showed that the proposed algorithm converges faster, and results in higher throughput at the same time. Since the proposed solution provides flexibility

in terms of choosing the constraint on the IRS reflection coefficients, it opens up the possibility of solving the joint optimization problem using more physically realistic models for the IRS reflection elements. The optimality of the VAMP-based solution can also be investigated through state evolution analysis. For non-convex optimization problems like optimizing the phase shifter matrix under unimodular constraint, the proposed solution might be asymptotically (for large matrix sizes) optimal if the proximal functions (i.e.,  $g_2$  and  $g'_2$ ) are Lipschitz continuous and the state evolution analysis reveals that the VAMP-based algorithm has only one fixed point [30].

## APPENDIX A

We solve the following optimization problem:

$$\arg \min_{\chi} f(\chi), \quad (59)$$

where

$$f(\chi) \triangleq \left| \tilde{r} - \frac{1}{1 + j\chi} \right|^2, \quad (60)$$

where  $\chi \in \mathbb{R}$  and  $\tilde{r} \in \mathbb{C}$ . Expanding the objective function, we re-express it as follows:

$$\arg \min_{\chi} \tilde{r}^* \tilde{r} - \frac{\tilde{r}^*}{1 + j\chi} - \frac{\tilde{r}}{1 - j\chi} + \frac{1}{(1 - j\chi)(1 + j\chi)}. \quad (61)$$

Let  $a \triangleq \Re\{\tilde{r}\}$  and  $b \triangleq \Im\{\tilde{r}\}$ . We substitute  $a$  and  $b$  into equation (61) and simplify the objective function as:

$$\arg \min_{\chi} a^2 + b^2 + \frac{1 - 2a}{1 + \chi^2} + \frac{2b\chi}{1 + \chi^2}. \quad (62)$$

We define  $c \triangleq (1 - 2a)$  and take the derivative w.r.t.  $\chi$  and equate it to zero to get the following expression:

$$f'(\chi) = \frac{2b(1 - \chi^2)}{(1 + \chi^2)^2} - \frac{2c\chi}{(1 + \chi^2)^2} = 0. \quad (63)$$

Simplifying the equation in (63) we get:

$$b\chi^2 + c\chi - b = 0. \quad (64)$$

The roots of the quadratic equation in (64) are real and distinct and given as under:

$$\chi_1 = \frac{-c - \sqrt{c^2 + 4b^2}}{2b}. \quad (65)$$

and

$$\chi_2 = \frac{-c + \sqrt{c^2 + 4b^2}}{2b}, \quad (66)$$

where  $b \neq 0$ . We take the second derivative w.r.t.  $\chi$  and after simplifications we have the following expression:

$$f''(\chi) = \frac{2}{(1 + \chi^2)^3} (2b\chi^3 - 6b\chi + 3c\chi^2 - c). \quad (67)$$

Substituting  $\chi = \chi_1$  in equation (67) and simplifying the result we get:

$$f''(\chi_1) = \frac{1}{(1 + \chi_1^2)^3} \left( \frac{1}{b^2} \left( c^3 + c^2\sqrt{c^2 + 4b^2} \right) + 4 \left( c + \sqrt{c^2 + 4b^2} \right) \right). \quad (68)$$

Since  $b \neq 0$ , therefore we have  $c^2\sqrt{c^2 + 4b^2} > |c^3|$  and  $\sqrt{c^2 + 4b^2} > |c|$  which implies that  $f''(\chi_1) > 0$ . Similarly, we have:

$$f''(\chi_2) = \frac{1}{(1 + \chi_2^2)^3} \left( \frac{1}{b^2} \left( c^3 - c^2\sqrt{c^2 + 4b^2} \right) + 4 \left( c - \sqrt{c^2 + 4b^2} \right) \right) < 0, \quad b \neq 0. \quad (69)$$

Thus, we choose:

$$\chi^{\text{opt}} = \chi_1 = \frac{-(1 - 2a) - \sqrt{(1 - 2a)^2 + 4b^2}}{2b}, \quad (70)$$

Interestingly, the solution,  $\chi_1$ , results in the same sign for  $\Im\{(1 + j\chi_1)^{-1}\}$  as  $\Im\{\tilde{r}\}$ .

## REFERENCES

- [1] F. Rusek, D. Persson, B. K. Lau, E. G. Larsson, T. L. Marzetta, O. Edfors, and F. Tufvesson, “Scaling up MIMO: Opportunities and challenges with very large arrays,” *IEEE Signal Processing Magazine*, vol. 30, no. 1, pp. 40–60, 2012.
- [2] E. G. Larsson, O. Edfors, F. Tufvesson, and T. L. Marzetta, “Massive MIMO for next generation wireless systems,” *IEEE Communications Magazine*, vol. 52, no. 2, pp. 186–195, 2014.
- [3] T. L. Marzetta, “Noncooperative cellular wireless with unlimited numbers of base station antennas,” *IEEE Transactions on Wireless Communications*, vol. 9, no. 11, pp. 3590–3600, 2010.
- [4] S. Buzzi, I. Chih-Lin, T. E. Klein, H. V. Poor, C. Yang, and A. Zappone, “A survey of energy-efficient techniques for 5G networks and challenges ahead,” *IEEE Journal on Selected Areas in Communications*, vol. 34, no. 4, pp. 697–709, 2016.
- [5] S. Zhang, Q. Wu, S. Xu, and G. Y. Li, “Fundamental green tradeoffs: Progresses, challenges, and impacts on 5G networks,” *IEEE Communications Surveys & Tutorials*, vol. 19, no. 1, pp. 33–56, 2016.
- [6] X. Tan, Z. Sun, D. Koutsonikolas, and J. M. Jornet, “Enabling indoor mobile millimeter-wave networks based on smart reflect-arrays,” in *IEEE Conference on Computer Communications (INFOCOM)*, 2018, pp. 270–278.
- [7] C. Liaskos, S. Nie, A. Tsoliariadou, A. Pitsillides, S. Ioannidis, and I. Akyildiz, “A new wireless communication paradigm through software-controlled metasurfaces,” *IEEE Communications Magazine*, vol. 56, no. 9, pp. 162–169, 2018.
- [8] S. Hu, F. Rusek, and O. Edfors, “Beyond massive MIMO: The potential of data transmission with large intelligent surfaces,” *IEEE Transactions on Signal Processing*, vol. 66, no. 10, pp. 2746–2758, 2018.
- [9] C. Pan, H. Ren, K. Wang, W. Xu, M. Elkashlan, A. Nallanathan, and L. Hanzo, “Multicell MIMO communications relying on intelligent reflecting surfaces,” *IEEE Transactions on Wireless Communications*, vol. 19, no. 8, pp. 5218–5233, 2020.
- [10] Q. Wu and R. Zhang, “Intelligent reflecting surface enhanced wireless network via joint active and passive beamforming,” *IEEE Transactions on Wireless Communications*, vol. 18, no. 11, pp. 5394–5409, 2019.

- [11] C. Huang, A. Zappone, G. C. Alexandropoulos, M. Debbah, and C. Yuen, “Reconfigurable intelligent surfaces for energy efficiency in wireless communication,” *IEEE Transactions on Wireless Communications*, vol. 18, no. 8, pp. 4157–4170, 2019.
- [12] Q. Wu and R. Zhang, “Beamforming optimization for wireless network aided by intelligent reflecting surface with discrete phase shifts,” *IEEE Transactions on Communications*, vol. 68, no. 3, pp. 1838–1851, 2019.
- [13] G. Zhou, C. Pan, H. Ren, K. Wang, and A. Nallanathan, “A framework of robust transmission design for IRS-aided MISO communications with imperfect cascaded channels,” *IEEE Transactions on Signal Processing*, vol. 68, pp. 5092–5106, 2020.
- [14] H. Guo, Y.-C. Liang, and S. Xiao, “Model-free optimization for reconfigurable intelligent surface with statistical CSI,” *arXiv preprint, arXiv:1912.10913*, 2019.
- [15] X. Yu, D. Xu, and R. Schober, “Optimal beamforming for MISO communications via intelligent reflecting surfaces,” in *IEEE 21st International Workshop on Signal Processing Advances in Wireless Communications (SPAWC)*. IEEE, 2020, pp. 1–5.
- [16] P. Wang, J. Fang, X. Yuan, Z. Chen, and H. Li, “Intelligent reflecting surface-assisted millimeter wave communications: Joint active and passive precoding design,” *IEEE Transactions on Vehicular Technology*, 2020.
- [17] S. Abeywickrama, R. Zhang, Q. Wu, and C. Yuen, “Intelligent reflecting surface: Practical phase shift model and beamforming optimization,” *IEEE Transactions on Communications*, vol. 68, no. 9, pp. 5849–5863, 2020.
- [18] Q.-U.-A. Nadeem, A. Kammoun, A. Chaaban, M. Debbah, and M.-S. Alouini, “Asymptotic analysis of large intelligent surface assisted MIMO communication,” *ArXiv*, vol. abs/1903.08127, 2019.
- [19] Y. Li, M. Jiang, Q. Zhang, and J. Qin, “Joint beamforming design in multi-cluster MISO NOMA reconfigurable intelligent surface-aided downlink communication networks,” *IEEE Transactions on Communications*, vol. 69, no. 1, pp. 664–674, 2021.
- [20] D. P. Bertsekas, “Nonlinear programming,” *Journal of the Operational Research Society*, vol. 48, no. 3, pp. 334–334, 1997.
- [21] S. Rangan, P. Schniter, and A. K. Fletcher, “Vector approximate message passing,” *IEEE Transactions on Information Theory*, vol. 65, no. 10, pp. 6664–6684, 2019.
- [22] R. W. Heath Jr. and A. Lozano, *Foundations of MIMO Communication*. Cambridge University Press, 2018.
- [23] Dongning Guo, S. Shamai, and S. Verdu, “Mutual information and minimum mean-square error in Gaussian channels,” *IEEE Transactions on Information Theory*, vol. 51, no. 4, pp. 1261–1282, 2005.
- [24] A. Manoel, F. Krzakala, G. Varoquaux, B. Thirion, and L. Zdeborová, “Approximate message-passing for convex optimization with non-separable penalties,” *arXiv preprint arXiv:1809.06304*, 2018.
- [25] D. L. Donoho, A. Maleki, and A. Montanari, “Message passing algorithms for compressed sensing: I. motivation and construction,” in *IEEE Information Theory Workshop on Information Theory (ITW 2010, Cairo)*, 2010, pp. 1–5.
- [26] C. M. Bishop, *Pattern Recognition and Machine Learning*. Springer, 2006.
- [27] M. Bayati and A. Montanari, “The dynamics of message passing on dense graphs, with applications to compressed sensing,” *IEEE Transactions on Information Theory*, vol. 57, no. 2, pp. 764–785, 2011.
- [28] M. Joham, W. Utschick, and J. A. Nossek, “Linear transmit processing in MIMO communications systems,” *IEEE Transactions on Signal Processing*, vol. 53, no. 8, pp. 2700–2712, 2005.
- [29] A. Sinha, P. Malo, and K. Deb, “A review on bilevel optimization: From classical to evolutionary approaches and applications,” *IEEE Transactions on Evolutionary Computation*, vol. 22, no. 2, pp. 276–295, 2018.
- [30] J. Barbier, F. Krzakala, N. Macris, L. Miolane, and L. Zdeborová, “Optimal errors and phase transitions in high-dimensional generalized linear models,” *Proceedings of the National Academy of Sciences*, vol. 116, no. 12, pp. 5451–5460, 2019.